



## Self-ordered particle trains in inertial microchannel flows

Yanfeng Gao, Pascale Magaud, Lucien Baldas, Christine Lafforgue, Micheline Abbas, Stéphane Colin

### ► To cite this version:

Yanfeng Gao, Pascale Magaud, Lucien Baldas, Christine Lafforgue, Micheline Abbas, et al.. Self-ordered particle trains in inertial microchannel flows. *Microfluidics and Nanofluidics*, 2017, 21 (10), pp.154. 10.1007/s10404-017-1993-5 . hal-01816577

**HAL Id: hal-01816577**

**<https://hal.science/hal-01816577>**

Submitted on 11 Oct 2018

**HAL** is a multi-disciplinary open access archive for the deposit and dissemination of scientific research documents, whether they are published or not. The documents may come from teaching and research institutions in France or abroad, or from public or private research centers.

L'archive ouverte pluridisciplinaire **HAL**, est destinée au dépôt et à la diffusion de documents scientifiques de niveau recherche, publiés ou non, émanant des établissements d'enseignement et de recherche français ou étrangers, des laboratoires publics ou privés.




## Open Archive Toulouse Archive Ouverte

OATAO is an open access repository that collects the work of Toulouse researchers and makes it freely available over the web where possible

This is an author's version published in: <http://oatao.univ-toulouse.fr/20416>

**Official URL:** <https://doi.org/10.1007/s10404-017-1993-5>

**To cite this version:**

Gao, Yanfeng and Magaud, Pascale and Baldas, Lucien and Lafforgue, Christine and Abbas, Micheline  and Colin, Stéphane *Self-ordered particle trains in inertial microchannel flows*. (2017) *Microfluidics and Nanofluidics*, 21 (10). ISSN 1613-4982

Any correspondence concerning this service should be sent  
to the repository administrator: [tech-oatao@listes-diff.inp-toulouse.fr](mailto:tech-oatao@listes-diff.inp-toulouse.fr)

# Self-ordered particle trains in inertial microchannel flows

Yanfeng Gao<sup>1</sup> · Pascale Magaud<sup>1</sup> · Lucien Baldas<sup>1</sup> · Christine Lafforgue<sup>2</sup> ·  
Micheline Abbas<sup>3</sup> · Stéphane Colin<sup>1</sup>

**Abstract** Controlling the transport of particles in flowing suspensions at microscale is of interest in numerous contexts such as the development of miniaturized and point-of-care analytical devices (in bioengineering, for foodborne illnesses detection, etc.) and polymer engineering. In square micro-channels, neutrally buoyant spherical particles are known to migrate across the flow streamlines and concentrate at specific equilibrium positions located at the channel centerline at low flow inertia and near the four walls along their symmetry planes at moderate Reynolds numbers. Under specific flow and geometrical conditions, the spherical particles are also found to line up in the flow direction and form evenly spaced trains. In order to statistically explore the dynamics of train formation and their dependence on the physical parameters of the suspension flow (particle-to-channel size ratio, Reynolds number and solid volume fraction), experiments have been conducted based on in situ visualizations of the flowing particles by optical microscopy. The trains form only once particles have reached their equilibrium positions (following lateral migration). The percentage of particles in trains and the interparticle distance in a train have been extracted and analyzed. The percentage of particles organized in trains increases with the particle Reynolds number

up to a threshold value which depends on the concentration and then decreases for higher values. The average distance between the surfaces of consecutive particles in a train decreases as the particle Reynolds number increases and is independent of the particles size and concentration, if the concentration remains below a threshold value related to the degree of confinement of the suspension flow.

**Keywords** Microfluidics · Inertial focusing · Train of particles · Hydrodynamic self-assembly

## 1 Introduction

Focusing particles into a tight stream is usually a necessary step prior to their counting, detecting or sorting, which is useful in many areas such as agriculture, biomedicine, environment, food technology or pharmaceutical industry. Various particle focusing methods have been developed for microfluidic applications, most of them requiring sheath flows and/or an outer force field that complicate their fabrication and miniaturization, increase the cost, require large sample volumes and could damage living bio-cells (Pamme 2007). Thus, developing sheath-free passive miniaturized focusing systems is of major interest due to their lower fabrication costs, lower sample volumes, adaptability to automation and easy portability.

In the last decade, particle migration due to flow inertia has been extensively used for successful particle focusing in microfluidic devices. Under specific flow and geometrical conditions, flowing particles can naturally migrate due to flow inertia to equilibrium positions where they concentrate. The trend of particles toward migration across the flow streamlines, first described in circular tubes by Poiseuille (1836), was later confirmed by the experiments of Segre and

---

✉ Lucien Baldas  
lucien.baldas@insa-toulouse.fr

<sup>1</sup> Institut Clément Ader (ICA), INSA, ISAE-SUPAERO, Mines-Albi, UPS, Université de Toulouse, 3 rue Caroline Aigle, 31400 Toulouse, France

<sup>2</sup> Laboratoire d'Ingénierie des Systèmes Biologiques et des Procédés (LISBP), CNRS, INRA, INSA, Université de Toulouse, 135 avenue de Rangueil, 31077 Toulouse, France

<sup>3</sup> Laboratoire de Génie Chimique (LGC), CNRS, INPT, UPS, Université de Toulouse, 4 allée Emile Monso, 31432 Toulouse, France

Silberberg (1962), then in many microfluidic experiments (Di Carlo et al. 2007; Bhagat et al. 2008; Choi et al. 2011). The phenomenon of inertial particle migration was theoretically explained at small particle Reynolds numbers (Saffman 1965; Ho and Leal 1974; Vasseur and Cox 1976) and then extended to finite particle Reynolds numbers (Schonberg and Hinch 1989; Asmolov 1999; Hood et al. 2015). With the development of powerful simulation tools, particle migration and their equilibrium positions were numerically investigated in square and circular channel flows (Chun and Ladd 2006; Shao et al. 2008; Di Carlo et al. 2009; Abbas et al. 2014). Segre and Silberberg (1962) mentioned that the particles not only migrate to equilibrium positions within a cross section, but also become ordered or evenly spaced in the flow direction. This inertial ordering of particles in trains has been experimentally observed both in circular ducts where particles migrate toward an annulus close to the wall (Matas et al. 2004) and in rectangular microchannels (Hur et al. 2010). In curved rectangular microchannels, Martel and Toner (2013) have also observed trains of particles occurring on the focusing lines whose positions are shown to be controlled by three non-dimensional numbers: Reynolds and Dean numbers and confinement ratio.

The particle self-ordering opens the possibility of manipulating particle positions not only in the spanwise but also in the streamwise direction, which could lead to a platform for a complete control, in the three spatial dimensions, of particle positions in a flow. Such a microfluidic device could be used in a broad spectrum of applications (Lee et al. 2010). For example, more uniform and controlled particle distributions improve the efficiency of flow cytometry (Oakey et al. 2010), single-cell encapsulation (Edd et al. 2008) and cell diagnostics (Hur et al. 2010).

Hydrodynamic interactions between particles were identified as underlying forces acting in the train formation. This has been summarized in Amini et al. (2014) in the context of inertial focusing. Whereas the streamlines around an isolated sphere in a pure shear flow are either open or completely closed under Stokes flow conditions, both flow inertia and confinement (presence of walls) can lead to the appearance of reversing streamlines around a single particle. Numerical simulations have shown that the trajectories of a second particle with respect to a reference one are relatively similar to the streamlines around a single particle, in pure shear (Kulkarni and Morris 2008; Haddadi and Morris 2015) as well as in channel (Humphry et al. 2010) flows. The latter study considered the motion of a pair of spheres that were initially separated by a given distance along the flow direction and located on their inertial focusing lines. The two particles moved closer following a damped oscillatory trajectory and eventually reached a steady axial spacing. This oscillatory motion through which stable self-assembled pairs are formed was experimentally observed by Lee et al. (2010)

using high-speed imaging. Based on these observations, Lee et al. (2010) suggested a mechanism for the dynamic self-assembly process: Due to an interplay between the viscous disturbance flow, which deviates the particles from inertial focusing lines, and the inertial lift force, which tends to restore the particle location, the average spacing between particles changes until it reaches an equilibrium value downstream in the channel. These authors also observed that the dynamics of more than two particles mainly follows the same mechanism: The train grows as additional particles join already organized particle pairs or trains of particles, and particle–particle interactions within a train, evidenced by oscillations and acceleration patterns during interaction, are essentially the same as in two-particle interactions. In the context of multi-particle interactions, Kahkeshani et al. (2016) showed that the suspension concentration impacted the most probable spacing between particles in trains. If the disturbance streamlines around a single particle are affected by the presence of other particles, the fundamental description of the flow leading to train formation remains an open question for future investigations.

Although the underlying mechanism that leads to particle organization in trains was recently elucidated, before the self-assembly process can be used in engineered microfluidic systems, several fundamental points still have to be explored:

- the simultaneity or time sequence of particle lateral focusing and longitudinal ordering is still an open question. This question is important in order to determine the channel length required to achieve a steady-state spacing;
- even though first attempts have been made to explain this self-assembly mechanism, there is not yet a full consensus on the role of the flow parameters and the geometric channel characteristics on the interparticle spacing;
- the percentage of particles in trains is a key parameter for characterizing a given configuration. It has rarely been studied. There is a real lack of statistical studies on the formation and evolution of trains.

To fill in this gap, the positions of particles in a square channel are statistically explored in the present work, using *in situ* flow visualization. Square channels are used due to their easy manufacturing process and the possible focusing on only four precise lines at moderate Reynolds numbers (near each channel wall along their symmetry planes). Using relatively small particle-to-channel size ratios, the four “focalization positions” in a square channel are far enough from each other to avoid interactions between particles in trains at different equilibrium positions. It is discussed whether the trains form during particle migration or once the particles have reached the equilibrium positions in the cross section. Then, a systematic study on the effect of different

factors such as the distance from the channel inlet, volume fraction, channel Reynolds number  $Re$  and particle Reynolds number  $Re_p$  which are linked by the particle-to-channel size ratio (see Sect. 2.1) and on the percentage  $\psi$  of particles in trains and the interparticle distance  $l$  extracted from image analysis is presented.

## 2 Set up

### 2.1 Experimental method

The spherical particles used for this study are made of polystyrene (Interfacial Dynamics Corporation) with diameters  $d_p = 5.3$  and  $8.7 \mu\text{m}$  and a density  $\rho = 1050 \text{ kg m}^{-3}$ . The fluid density is matched to the particle one by using a mixture of 23% glycerol and 77% deionized water to prevent the sedimentation and particles are introduced at volume fractions  $\Phi = 0.02$  to 1%. The fluid kinematic viscosity  $\nu$  of such a mixture is about  $1.5 \times 10^{-6} \text{ m}^2/\text{s}$  at room temperature. The suspension is introduced in square borosilicate microchannels (Vitrocom) with an  $80 \times 80 \mu\text{m}^2$  inner section and 10, 30 and 60 cm lengths, linked at the inlet with a silicone tube of inner diameter 0.81 mm by a conic junction. The micro-flow is generated by a syringe pump (PDH 4400, Harvard Apparatus) at flow rates ranging from 8.3 nL/s to 33  $\mu\text{L/s}$  corresponding to  $Re = 0.07$  to 280 (the channel Reynolds number is defined by  $Re = UH/\nu$  where  $U$  is the mean flow velocity and  $H$  the channel hydraulic diameter which is here also the channel height). Particle migration is visualized by an Olympus microscope (BX 51), and images are recorded with a frequency of 50 fps along the channel length by a high-speed camera (Photron Fastcam SA3) focused at the midplane of the channel. The exposure time is varied from 2 to 5  $\mu\text{s}$  depending on the flow rate, and at least 2000 images are captured to yield satisfactory results. The depth of field, calibrated by static particles monitoring, is about 10  $\mu\text{m}$ . A schematic diagram of the experimental setup is presented in Fig. 1a.

Figure 1b, c shows two examples of trains of particles at two different moderate Reynolds numbers and particle Reynolds numbers, defined as  $Re_p = Re (d_p/H)^2$ . The particles in Fig. 1b are bright, indicating their localization in the focal plane (in this figure in the midplane of the channel). In this example, the observed particles are aligned near the vertical walls in the horizontal symmetry plane of the channel and form two regular trains. In Fig. 1c, other trains of particles appear without bright points. They are out of the focal plane, in the vertical symmetry plane and apparently close to the bottom wall. These locations are consistent with the four expected inertial focusing equilibrium positions previously observed in square channels (Abbas et al. 2014).

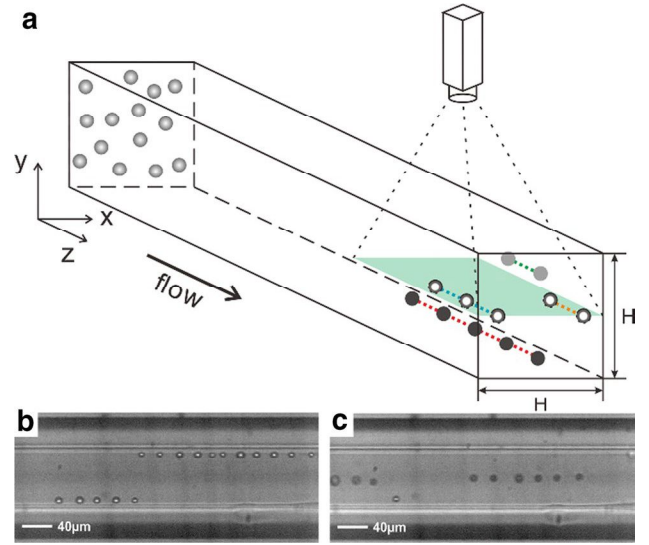


**Fig. 1** a Schematic diagram of the experimental setup. Examples of images of particle trains recorded at the channel midplane ( $y/H = 0.5$ ),  $z/H = 1000$ ,  $\Phi = 0.10\%$ , b  $Re = 210$  ( $Re_p = 2.48$ ) and c  $Re = 112$  ( $Re_p = 1.32$ )

### 2.2 Data processing

The original grayscale images are post-processed with Matlab<sup>®</sup>. First, images are rotated to optimally align  $x$ - and  $z$ -axes with the main axes of the figure (Fig. 2a) and a background subtraction operation is performed. Each image is then thresholded in order to obtain a binary image. Contours are extracted and selected depending on surface and shape so that particle positions are precisely determined. The  $x$  and  $z$  coordinates of each particle in the focal plane are then measured. Trains are identified when three or more particles are aligned with a regular interparticle spacing. In Fig. 2b, particles considered in trains are highlighted by the yellow rectangles, particles considered out of trains and in the focal plane are indicated by the red circles and particles out of the focal plane are indicated by the green triangles. The total number of particles in and out of trains is calculated over a set of 2000 images, and the percentage of particles in trains is thus evaluated. For this analysis, all particles are considered, whatever the value of their  $y$ -coordinate, i.e., either in or out of the focal plane. This percentage is underestimated since some trains are sliced in some images and might thus not be identified by the data processing method. Finally, the probability density function (PDF) of streamwise spacing  $l$  between centers of consecutive particles normalized by the particle diameter  $d_p$  is computed for particles observed in trains, and the highest peak is identified and chosen as a metrics of the most probable spacing between consecutive

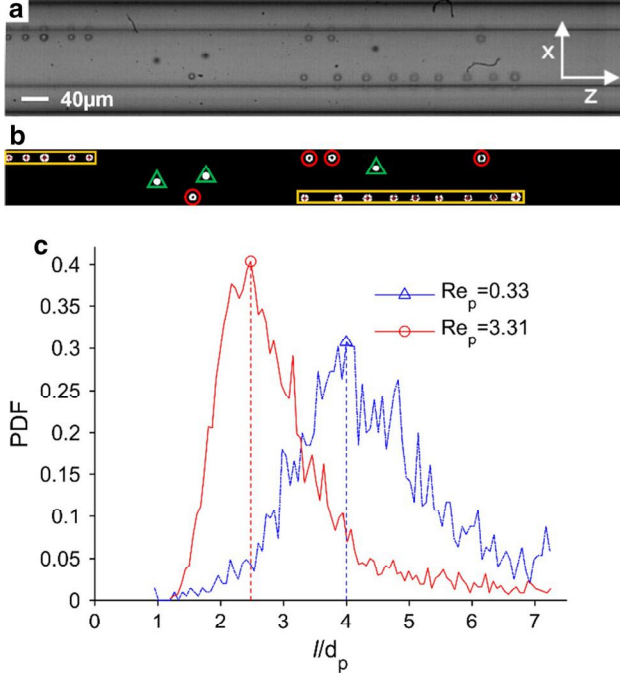


**Fig. 2** **a** Original grayscale image after rotation. **b** Post-processed image where particles in trains are highlighted in rectangles. **c** PDF of normalized interparticle spacing for  $Re_p = 0.33$  and  $3.31$ ,  $\Phi = 0.10\%$  and  $z/H = 1000$

particles in trains. The PDF of the axial spacing between particles at  $\Phi = 0.10\%$ ,  $Re_p = 0.33$  and  $3.31$  (corresponding to  $Re = 28$  and  $280$ ) and  $z/H = 1000$  are presented in Fig. 2c.

In these two examples, the most probable spacing between consecutive particles in trains is thus determined as  $l/d_p = 4$  for  $Re_p = 0.33$  and  $l/d_p = 2.5$  for  $Re_p = 3.31$ .

### 3 Results and discussion

#### 3.1 Dynamics of train formation

The percentage  $\psi$  of particles in trains and the normalized interparticle distance  $l/d_p$  are studied as functions of the normalized distance from the channel inlet  $z/H$ , in Fig. 3a, b for  $d_p/H = 0.11$ ,  $\Phi = 0.10\%$  and different values of  $Re_p$ . Long channels (60 cm long) are used at low particle Reynolds number ( $Re_p = 0.07$ ) in order to allow particles to reach their focusing position (channel centerline); medium channels (30 cm) and short channels (10 cm) are used for  $Re_p = 0.13$  and  $Re_p = 0.33$  or  $1.32$ , respectively, to limit pressure losses.

Under the current experimental conditions, the percentage  $\psi$  of particles in trains increases when moving downstream in the channel, indicating that trains form progressively (Fig. 3a). None of the obtained curves seems to have reached a stable level, indicating that some particles certainly still join the existing trains or form new ones even far from the channel inlet ( $z/H = 7125$  for low  $Re_p$  and  $z/H = 1000$  for higher  $Re_p$ ). This suggests that train formation is a slow phenomenon. The interparticle distance nevertheless becomes rapidly almost constant along the channel, but its value depends on the value of  $Re_p$  (Fig. 3b). It can be noted that this result is different from that obtained by Lee et al. (2010) who observed that the interparticle spacing continuously increased along the channel.

Since particles are “simultaneously” laterally focused and longitudinally ordered in trains while traveling downstream in the channel, it seems important to investigate the relationship between these two phenomena. It is well known that particles migrate in a square channel following a two-stage process (Choi et al. 2011; Abbas et al. 2014). In the first stage, they undergo a cross-streamline migration orthogonal

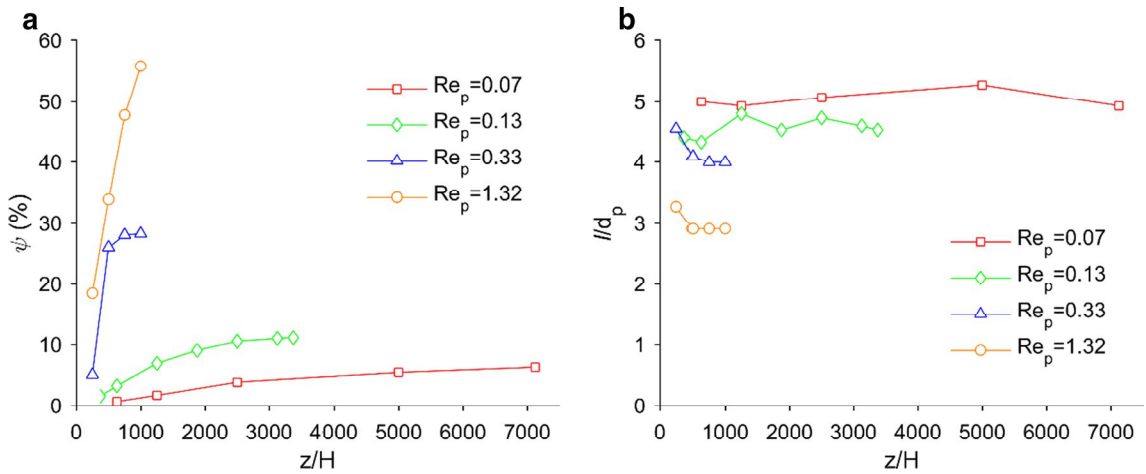


**Fig. 3** **a** Percentage  $\psi$  of particles in trains and **b** normalized interparticle distance  $l/d_p$  as functions of the normalized distance  $z/H$  from channel inlet for  $d_p/H = 0.11$ ,  $\Phi = 0.10\%$  and different values of the particle Reynolds number  $Re_p$



to the velocity iso-contours until they reach an equilibrium ring close to the channel perimeter, followed by a cross-lateral motion along the equilibrium ring (parallel to the wall) toward one of the four final equilibrium positions located on the symmetry planes of the channel walls. Probability density functions of particles detected in the focal plane at  $y/H = 0.5$  (solid red lines) and across the whole channel depth (dotted blue lines) are both displayed in Fig. 4 versus the normalized transverse direction  $x/H$ , for the same experimental conditions as described in Fig. 3. Schematic representations of particle distributions in the cross section are also proposed (deduced from other PDF obtained at different heights  $y/H$  and not presented in this work).

At low flow inertia (typically  $Re_p < 10^{-2}$ ), Abbas et al. (2014) have highlighted a second regime of migration in which particles concentrate in the channel center. At  $Re_p = 0.07$  and  $z/H = 7125$ , particles are found on the channel centerline and on an annulus close to the walls, indicating the coexistence of the two regimes of migration, observed at low (toward the channel centerline) and moderate (toward four equilibrium positions near the center of the channel faces) Reynolds numbers. At  $Re_p = 0.13$  ( $z/H = 3375$ ) and

$Re_p = 0.33$  ( $z/H = 250$ ), particles are concentrated on a ring almost parallel to the channel walls, indicating that they are in the first stage (lateral migration) of their migration at moderate Reynolds numbers. At  $Re_p = 0.33$  ( $z/H = 500$  and  $1000$ ), all the particles have focused along the channel perimeter, according to the first stage of the migration process, but they have not all reached the four final equilibrium positions. On the contrary, at  $Re_p = 1.32$  and  $z/H = 1000$ , the two stages of the migration are fully completed. However, the trendline of train formation for this case still increases (see Fig. 3), which seems to show that the longitudinal ordering process is slower, or starts later, than the lateral migration process.

Another important question concerns the starting point of the self-assembly process: Does this process start during the lateral migration of the particles or only once these particles are focused on their final equilibrium positions?

All in-focus particles centers extracted from 2000 images are superimposed in a single image in Fig. 5a, at  $Re_p = 0.13$  and  $z/H = 3375$ . They are detected in three focal planes located at different vertical heights;  $y/H = 0.5$  corresponds to the channel midplane and  $y/H = 0.15$  is close to the bottom

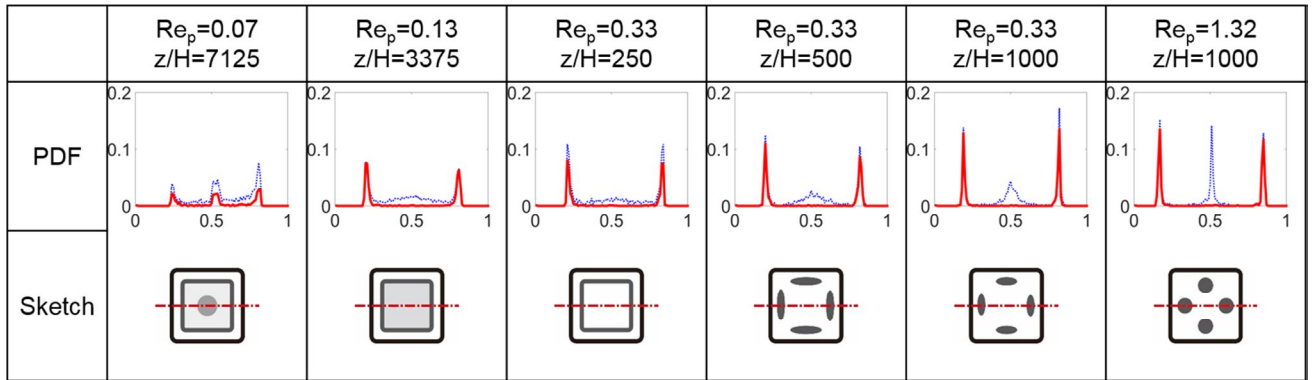


**Fig. 4** PDF of particles at  $y/H = 0.5$  (channel midplane), for  $\Phi = 0.10\%$ , different values of  $Re_p$  and  $z/H$ . Solid red lines correspond to particles in the focal plane and dotted blue ones to particles

present in the whole section. Distributions of particles in equilibrium are sketched below the PDF (color figure online)

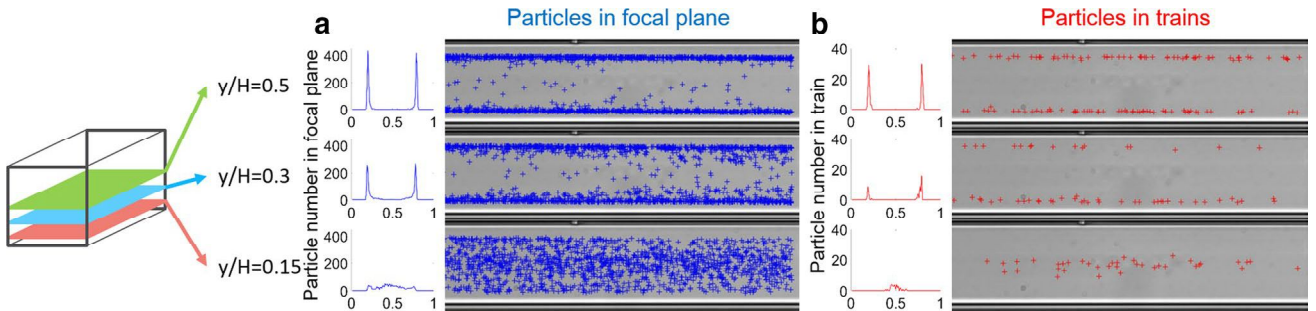


**Fig. 5** Particles **a** in focal plane (obtained from 2000 superimposed images) and **b** in trains at different vertical heights ( $y/H = 0.5, 0.3$  and  $0.15$ ) at  $Re_p = 0.13$ ,  $d_p/H = 0.11$  and  $\Phi = 0.10\%$ . Each blue or red cross represents the center of one particle (color figure online)

wall. For each height, the particles in trains are also identified and shown separately in Fig. 5b. The distribution in the transverse direction of the number of particles assembled in trains in the focal plane is also illustrated by histograms.

At  $y/H = 0.5$ , particles in the focal plane are mostly located near the front and back channel walls while at  $y/H = 0.15$ , they occupy all the layers, confirming that in this configuration ( $Re_p = 0.13$  and  $z/H = 3375$ ), particles are concentrated in an annulus close to the channel perimeter. In the same time, particles in trains are found to be located near the front and the back walls in the channel midplane ( $y/H = 0.5$ ) and only near the center of the channel in the plane close to the bottom wall ( $y/H = 0.15$ ). Even if all the particles are focused on a ring, particles in trains are only located at the four final equilibrium positions near the walls on their symmetry planes. Similar results have been obtained for other values of  $Re_p$  and  $z/H$ , even near the channel inlet. Trains are thus found to be located only on the particle final focusing lines, indicating that the self-assembly process concerns only particles which have completed their cross-lateral migration.

### 3.2 Dependence of self-ordering on different parameters

The observations of trains of particles presented in this section are all recorded at the same distance from the channel inlet ( $z/H = 1000$ ). As shown in Sect. 3.1, the trains are formed at this position, for most of the experiments run at  $Re_p \geq 0.1$ .

#### 3.2.1 Effect of flow inertia and particle size

The percentage  $\psi$  of particles in trains is displayed with respect to the particle Reynolds number and the channel Reynolds number in Fig. 6a and its inset, respectively, for

two values of the particle diameter-to-channel hydraulic diameter ratio:  $d_p/H = 0.11$  (at  $\Phi = 0.10\%$ ) and  $d_p/H = 0.066$  (at  $\Phi = 0.02\%$ ). These two different volume fractions are set to ensure the same number of particles in a given volume. The error bars represent the amplitude of the variations observed in six experiments done for each operating condition, and the square and triangle symbols correspond to the mean value of  $\psi$ . The last data obtained for the highest value of the particle Reynolds number,  $Re_p = 3.33$ , could unfortunately not be reproduced, due to clogging problems.

It is observed that as  $Re_p$  increases, the percentage  $\psi$  of particles in trains first increases, reaches a maximum around  $Re_p = 1.8$  and decreases for higher particle Reynolds numbers. A similar dependence on  $Re_p$  has been observed in tube flows by Matas et al. (2004), with a stronger peak reported in that study. Since trains are found to be located only on the particle focalization lines, it is relevant to compare the percentage of particles in trains with the percentage of particles located at the four final equilibrium positions. The focusing degree  $\eta$  is the total percentage of particles focused at the four equilibrium positions, defined as rectangular zones of  $0.4d_p$  in width and bounded by the depth of field. In Fig. 6b, the focusing degree is plotted with respect to the particle Reynolds number for  $d_p/H = 0.11$  and  $\Phi = 0.1\%$ . It is observed that the focusing degree  $\eta$  also starts to increase with  $Re_p$ , reaches a maximum around  $Re_p = 1.8$  and decreases for higher particle Reynolds numbers. As the images are recorded at a constant distance from the channel inlet, the increase in the focusing degree for  $Re_p < 1.8$  is due to the shorter streamwise length required for focalization when the particle Reynolds number is increased (Abbas et al. 2014). For  $Re_p > 1.8$ , i.e.,  $Re > 154$ , we have experimentally observed an enlargement of the focusing zones, which could be due to a transition toward new equilibrium positions near the channel corners, numerically and experimentally observed by Nakagawa et al. (2015) for

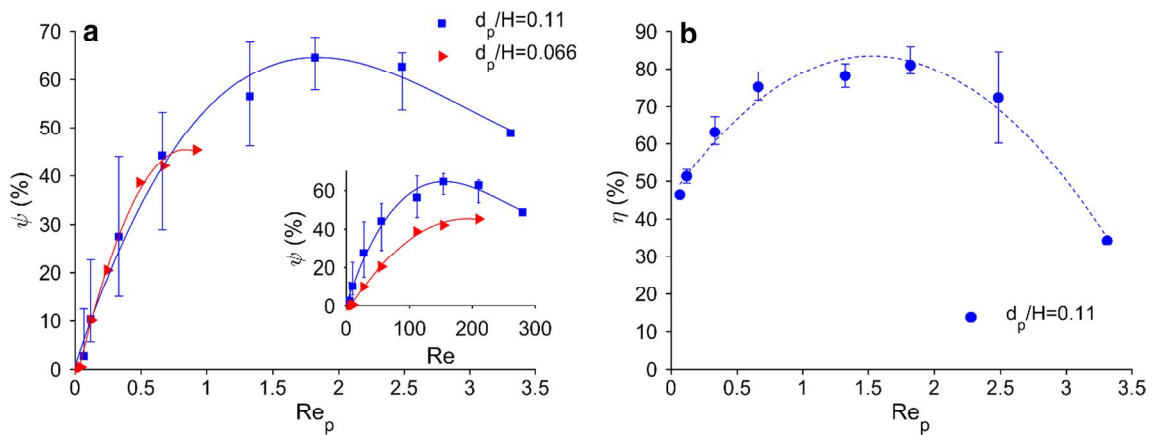


**Fig. 6** **a** Percentage  $\psi$  of particles in trains as a function of particle Reynolds number  $Re_p$  and channel Reynolds number  $Re$  (inset) for  $d_p/H = 0.11$  and  $d_p/H = 0.066$ . **b** Particle focusing degree  $\eta$  as a function of  $Re_p$  for  $d_p/H = 0.11$



channel Reynolds number above 260. This phenomenon could explain the decrease in the focusing degree observed for  $Re_p > 1.8$ .

The similarity in the evolutions of  $\psi$  and  $\eta$  (Fig. 6a, b) suggests that the percentage of particles in trains is constrained by the focusing degree of the suspension, i.e., when  $Re_p$  increases over its optimal value of 1.8, the enlargement of the focusing zones described above reduces the concentration of particles on the equilibrium positions and thus the probability for these particles to be trapped in trains. The increase in  $\psi$  is steeper than the increase in  $\eta$  for  $Re_p < 1$ ; this could be explained by the fact that when the particle Reynolds number increases, the region of reversing streamlines around a reference particle in a shear flow becomes wider (Mikulencak and Morris 2004; Kulkarni and Morris 2008; Haddadi and Morris 2015). This phenomenon favors the interparticle trapping and increases the number of particles in a train for a given concentration.

The percentage of particles in trains is higher for  $d_p/H = 0.11$  than for  $d_p/H = 0.066$  for the same channel Reynolds number (cf. inset of Fig. 6a), indicating that the particle confinement enhances the formation of trains. Moreover, these data collapse quite well onto a single curve (cf. Fig. 6a) when they are plotted as a function of the particle Reynolds number, suggesting that the particle ordering is controlled by the flow dynamics at the particle scale. These results are consistent with the data of Matas et al. (2004) obtained in circular pipe flow for  $Re$  between 0 and 3000. It is to be noticed that at the same confinement ( $d_p/H \sim 0.05$ ), the maximal proportion of particles in trains reaches 40% in square channel, whereas it reaches only 15% in a tube (Matas et al. 2004). The difference is certainly due to the fact that the equilibrium positions are restricted to four points in the cross section of a square channel flow, whereas they are distributed in a ring in a tube flow. Therefore, the probability of pair assembly is enhanced in the square channel flows.

The normalized interparticle distance in a train,  $l/d_p$ , defined as the distance between consecutive particle centers normalized by the particle diameter, is presented in Fig. 7 as a function of  $Re_p$ . The amplitude of the variations of  $l/d_p$  measured in six experiments done for each operating condition is always lower than 5%; error bars are thus not represented in this figure. In the range of particle Reynolds numbers considered here, the normalized interparticle distance decreases when  $Re_p$  increases. This is in agreement with the reports of Morris and co-authors (Mikulencak and Morris 2004; Kulkarni and Morris 2008; Haddadi and Morris 2015), who claimed that the distance between consecutive particles is set by the reversing streamline region around a particle in shear flow which gets closer to the reference particle surface when the particle Reynolds number increases.

The interparticle distance  $l/d_p$  is found to depend not only on the particle Reynolds number, but also on the degree of

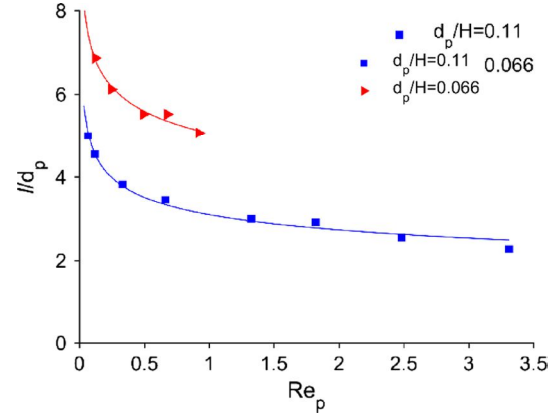


**Fig. 7** Normalized interparticle distance  $l/d_p$  as a function of particle Reynolds number  $Re_p$  for  $d_p/H = 0.11$  and  $d_p/H = 0.066$

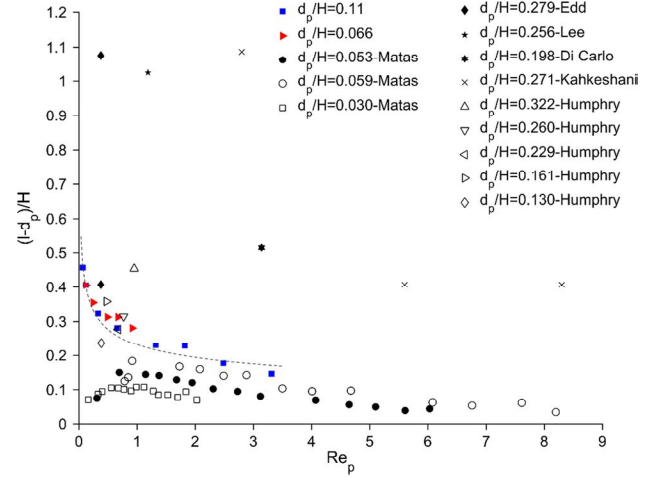


**Fig. 8** Normalized particle surface-to-surface spacing  $(l - d_p)/H$  as a function of particle Reynolds number  $Re_p$ : comparison between current results and data of Matas et al. (2004), Di Carlo et al. (2007), Edd et al. (2008), Humphry et al. (2010), Lee et al. (2010) and Kahkeshani et al. (2016). The dashed line is the trendline of the present experimental data (blue and red solid squares and triangles) (color figure online)

confinement (particle diameter-to-channel hydraulic diameter ratio). When the distance between the surfaces of two consecutive particles normalized by the channel hydraulic diameter,  $(l - d_p)/H$ , is plotted as a function of the particle Reynolds number (Fig. 8), the data obtained for the two different confinements (blue squares and red triangles) collapse quite well onto a single curve (dotted line in Fig. 8) which is not the case for  $l/d_p$ . More configurations, with various values of  $d_p/H$ , should be investigated to confirm this trend, but it can be already assumed that the key parameter is the distance between the surfaces of two consecutive particles rather than the distance between their centers. This is also confirmed by the data of Matas et al. (2004) reported in this

figure and obtained for similar weak degrees of confinement ( $d_p/H$  between 0.03 and 0.066), even if in this case  $(l - d_p)/H$  surprisingly increases with the flow inertia for low  $Re_p$ . Our data are also similar to those reported by Humphry et al. (2010) in a rectangular channel.

Other values of  $(l - d_p)/H$  are also reported in Fig. 8 for different experimental conditions. It can be seen that a high confinement ( $d_p/H > 0.2$ ) can lead to large interparticle spacing, as illustrated by the data of Edd et al. (2008), Lee et al. (2010), Di Carlo et al. (2007), Humphry et al. (2010) and Kahkeshani et al. (2016). These reported data, however, have all been obtained in specific configurations. Lee et al. (2010) and Kahkeshani et al. (2016) used a two-inlet co-flow within a rectangular channel, the particles being introduced in only one flow inlet. Using rectangular channels with high aspect ratio (leading to higher particle confinement), the particles were forced to align, in equilibrium, on a single line near the large wall on the side where the particles were introduced. In the case of one flow inlet and high channel aspect ratio, Edd et al. (2008) and Humphry et al. (2010) observed two classes of trains in equilibrium: Particles were either aligned along one side of the channel or observed alternatively near both largest walls. We also observed alternated trains in preliminary results obtained in rectangular channels with high aspect ratio. In highly confined channels, when a particle reaches its equilibrium position, it induces steady reversing streamlines near both walls [as illustrated in Humphry et al. (2010)] that highly impact relative particle trajectories. Due to the small dimensions of the channel, the reversing streamlines in the other half of the channel are sufficiently close to the particle to create either an alternated pair or a “single streamline” pair, depending on whether the second particle arrives on the same channel side or not. Edd et al. (2008) thus gave two interparticle distances, one for “single streamline” trains and one for alternated trains at the same  $Re_p$  (cf. Fig. 8). Di Carlo et al. (2007) observed that for highly confined flows in square channels, no more than one particle could be found in the same cross section, on one of the equilibrium positions. The resulting trains could be alternated or on a single focusing line.

At low flow inertia (typically  $Re_p < 10^{-2}$ ), particles concentrate in the channel centerline due to the so-called

shear-induced migration as highlighted by Abbas et al. (2014). Although the particles are gathered near the channel center for  $Re_p = 8 \times 10^{-4}$  and  $8 \times 10^{-3}$ , indicating that most of them have reached their equilibrium position, they are not regularly aligned as shown in Fig. 9, suggesting that no train is formed; some aggregates can also be observed.

As mentioned before, the particle pair formation is linked to the presence of reversing streamlines which also exist at low inertia and even for Stokes flow in confined configurations (Zurita-Gotor et al. 2007). In the pair interaction mechanism, these reversing streamlines initiate drag forces [reported as a viscous disturbance flow effect in Lee et al. (2010) or as a stresslet disturbance flow effect in Zurita-Gotor et al. (2007)] which push the two particles away from their focusing position, in spanwise opposite directions. Inertial lift forces direct then the particles back to the focusing line (Lee et al. 2010). This interplay between viscous disturbance flow effect and lift forces explains the oscillatory relative trajectories of the particles observed by these authors during the self-assembly process. However, the closed streamline regions around the particles expand when  $Re$  decreases, moving thus the reversing zones away from the particle (Haddadi and Morris 2015). In addition, the repulsive interaction initiated by the viscous disturbance flow decays with  $1/l^2$  (Zurita-Gotor et al. 2007; Lee et al. 2010) and thus decreases when the reversing zones move away from the particle as  $Re$  decreases. This could explain the vanishing of the self-assembly process observed at low inertia.

### 3.2.2 Effect of solid volume fraction

The influence of the particle volume fraction on the formation of trains is analyzed from the observations carried out at  $z/H = 1000$ , with a particle-to-channel size ratio  $d_p/H = 0.11$  and particle volume fractions  $\Phi$  ranging from 0.02 to 1%, as illustrated in Fig. 10.

For all considered concentrations, the evolution of the percentage of particles in trains with  $Re_p$  is similar: This percentage increases with  $Re_p$ , reaches a maximum and then decreases (Fig. 10a). When  $\Phi$  decreases, the maximum value of  $\psi$  decreases and the corresponding value of  $Re_p$  increases.

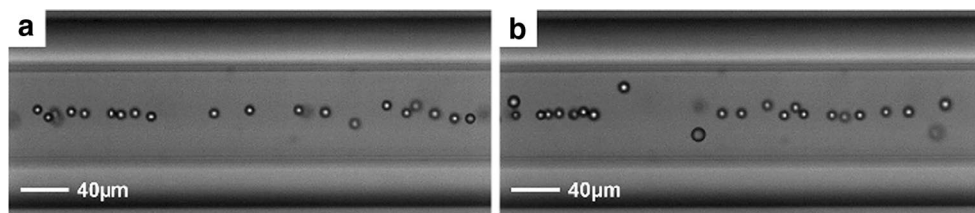


**Fig. 9** Snapshots of the suspension flow at low Reynolds numbers, taken at  $y/H = 0.5$ ,  $z/H = 1000$ ,  $\Phi = 0.4\%$ , **a**  $Re_p = 8 \times 10^{-4}$  ( $Re = 0.07$ ) and **b**  $Re_p = 8 \times 10^{-3}$  ( $Re = 0.7$ )

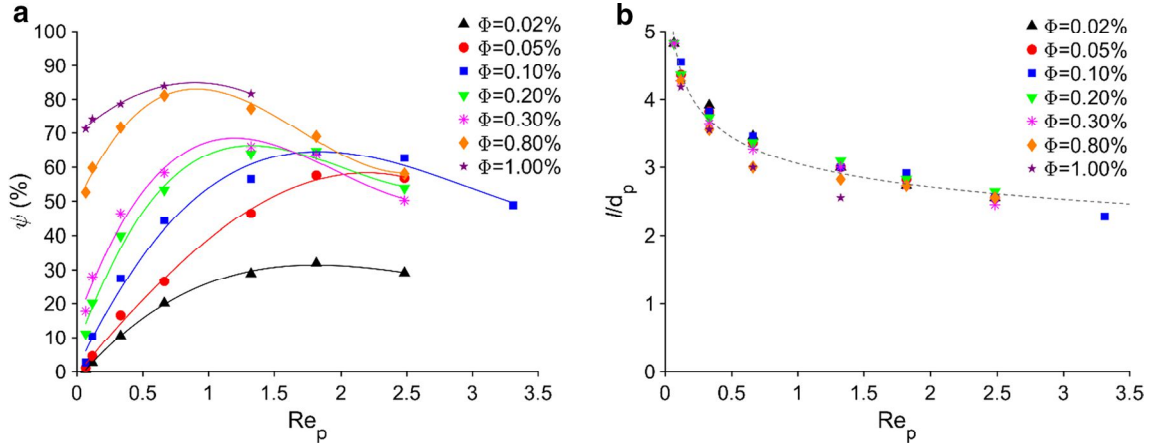


**Fig. 10** **a** Percentage of particles in trains  $\psi$  and **b** normalized interparticle distance  $l/d_p$  as a function of particle Reynolds number  $Re_p$  for  $d_p/H = 0.11$ ,  $z/H = 1000$  and  $\Phi = 0.02, 0.05, 0.1, 0.2, 0.3, 0.8$  and  $1\%$

It could be thus assumed that higher concentrations enhance particles self-assembly at small  $Re_p$ , which is no more the case at higher  $Re_p$  (around 2). Kahkeshani et al. (2016) also mentioned that at high concentrations, stable trains were no longer observed due to temporal fluctuations in interparticle spacing.

The interparticle distance decreases while increasing  $Re_p$  and turns out to be relatively independent of the concentration, as illustrated in Fig. 10b. Almost all the data obtained for different concentrations are well fitted by an exponential function (dashed line in the figure). However, a few points obtained for the highest concentrations, i.e.,  $\Phi = 0.8$  and  $1\%$ , are below the fitting curve. The number of particles per unit length or length fraction  $\lambda = 6\Phi(H^2/\pi d_p^3)$  was calculated to quantify the proximity between particles in the suspensions. If  $\lambda > 4/l$ , where 4 is the number of equilibrium positions in square channels, steric crowding effects, as defined by Di Carlo (2009), appear. Under the present experimental conditions,  $\lambda > 4/l$  is reached when  $\Phi = 0.8\%$  for  $Re_p < 1$  and when  $\Phi = 1\%$  for  $Re_p < 3$ . In that case, the interparticle distance decreases so that all particles can take place on one of the four equilibrium positions. This is confirmed by the experimental data presented in Fig. 10b. The diamond symbols representing  $\Phi = 0.8\%$  are located below the fitting line at  $Re_p = 0.33$  and  $0.66$ ; the same phenomenon for  $\Phi = 1\%$  represented by five-pointed star symbols is observed at  $Re_p = 0.33, 0.66$  and  $1.32$ . As long as the crowding limit is not reached, the interparticle distance is found to be independent of the concentration. Humphry et al. (2010) also found that the interparticle distance does not depend strongly on the volume fraction in rectangular microchannels. However, whenever the crowding limit was reached, they observed the formation of an additional train parallel to the original one located near the equilibrium position. It would

have been interesting to increase even more the particle concentration to check if such multiple parallel trains can be observed in square channels, but it was not possible due to the rapid clogging of the channel.

## 4 Conclusion

In this work, the formation of trains of particles in square microchannels has been experimentally studied. A statistical analysis of trains extracted from a large number of images, recorded and post-processed for various flow conditions and at various positions in the channel, has permitted to identify important relations between the structure of the trains (percentage of particles in trains and interparticle distance) and some flow conditions such as the particle Reynolds number and the particle concentration. It has been shown in particular that:

- the train formation process only starts when the particles have reached their equilibrium positions, located on four focusing lines close to the walls on their symmetry planes;
- high percentages of particles in trains can be reached in some flow configurations (up to 80% in the presently studied conditions);
- increasing the particle Reynolds number,  $Re_p$ , firstly favors the formation of trains, but leads to a diminution of the percentage of particles organized in trains over an optimal value of  $Re_p$ . With increasing concentrations, the maximal value of the percentage of particles in trains increases too and is reached for lower  $Re_p$  values;
- the distance between consecutive particles decreases when  $Re_p$  increases, independently of the particle concentration. However, if the concentration exceeds a thresh-

old value linked to the flow confinement (and defined as the crowding limit), the interparticle distance tends to decrease in relation to the concentration increase.

Even if these results allow a better understanding of the self-assembly mechanism, complementary works have to be performed to enable the design of new separation microdevices. In particular, the migration and self-assembly processes of non-spherical particles and poly-dispersed suspensions, closer to the biological suspensions that are found in some considered applications, have to be investigated.

**Acknowledgements** This work was partly supported by the Fédération de Recherche FERMAT, FR 3089 and the China Scholarship Council.

## References

- Abbas M, Magaud P, Gao Y, Geoffroy S (2014) Migration of finite sized particles in a laminar square channel flow from low to high Reynolds numbers. *Phys Fluids* 26:123301
- Amini H, Lee W, Di Carlo D (2014) Inertial microfluidic physics. *Lab Chip* 14:2739–2761
- Asmolov ES (1999) The inertial lift on a spherical particle in a plane Poiseuille flow at large channel Reynolds number. *J Fluid Mech* 381:63–87
- Bhagat AAS, Kuntaegowdanahalli SS, Papautsky I (2008) Inertial microfluidics for continuous particle filtration and extraction. *Microfluid Nanofluid* 7:217–226
- Choi YS, Seo KW, Lee SJ (2011) Lateral and cross-lateral focusing of spherical particles in a square microchannel. *Lab Chip* 11:460–465
- Chun B, Ladd A (2006) Inertial migration of neutrally buoyant particles in a square duct: an investigation of multiple equilibrium positions. *Phys Fluids* 18:031704
- Di Carlo D (2009) Inertial microfluidics. *Lab Chip* 9:3038–3046
- Di Carlo D, Irimia D, Tompkins RG, Toner M (2007) Continuous inertial focusing, ordering, and separation of particles in microchannels. *Proc Natl Acad Sci* 104:18892–18897
- Di Carlo D, Edd JF, Humphry KJ, Stone HA, Toner M (2009) Particle segregation and dynamics in confined flows. *Phys Rev Lett* 102:094503
- Edd JF, Di Carlo D, Humphry KJ, Koster S, Irimia D, Weitz DA, Toner M (2008) Controlled encapsulation of single-cells into monodisperse picolitre drops. *Lab Chip* 8:1262–1264
- Haddadi H, Morris JF (2015) Topology of pair-sphere trajectories in finite inertia suspension shear flow and its effects on microstructure and rheology. *Phys Fluids* 27:043302
- Ho B, Leal L (1974) Inertial migration of rigid spheres in two-dimensional unidirectional flows. *J Fluid Mech* 65:365–400
- Hood K, Lee S, Roper M (2015) Inertial migration of a rigid sphere in three-dimensional Poiseuille flow. *J Fluid Mech* 765:452–479
- Humphry KJ, Kulkarni PM, Weitz DA, Morris JF, Stone HA (2010) Axial and lateral particle ordering in finite Reynolds number channel flows. *Phys Fluids* 22:081703
- Hur SC, Tse HT, Di Carlo D (2010) Sheathless inertial cell ordering for extreme throughput flow cytometry. *Lab Chip* 10:274–280
- Kahkeshani S, Haddadi H, Di Carlo D (2016) Preferred interparticle spacings in trains of particles in inertial microchannel flows. *J Fluid Mech* 786:R3
- Kulkarni PM, Morris JF (2008) Pair-sphere trajectories in finite-Reynolds-number shear flow. *J Fluid Mech* 596:413–435
- Lee W, Amini H, Stone HA, Di Carlo D (2010) Dynamic self-assembly and control of microfluidic particle crystals. *Proc Natl Acad Sci USA* 107:22413–22418
- Martel JM, Toner M (2013) Particle Focusing in Curved Microfluidic Channels. *Scientific Reports* 3
- Matas J-P, Glezer V, Guazzelli É, Morris JF (2004) Trains of particles in finite-Reynolds-number pipe flow. *Phys Fluids* 16:4192–4195
- Mikulencak DR, Morris JF (2004) Stationary shear flow around fixed and free bodies at finite Reynolds number. *J Fluid Mech* 520:215–242
- Nakagawa N, Yabu T, Otomo R, Kase A, Makino M, Itano T, Sugihara-Seki M (2015) Inertial migration of a spherical particle in laminar square channel flows from low to high Reynolds numbers. *J Fluid Mech* 779:776–793
- Oakey J, Applegate RW Jr, Arellano E, Di Carlo D, Graves SW, Toner M (2010) Particle focusing in staged inertial microfluidic devices for flow cytometry. *Anal Chem* 82:3862–3867
- Pamme N (2007) Continuous flow separations in microfluidic devices. *Lab Chip* 7:1644–1659
- Poiseuille J (1836) Observations of blood flow. *Ann Sci Nat Srie* 5:1836
- Saffman P (1965) The lift on a small sphere in a slow shear flow. *J Fluid Mech* 22:385–400
- Schonberg JA, Hinch E (1989) Inertial migration of a sphere in Poiseuille flow. *J Fluid Mech* 203:517–524
- Segre G, Silberberg A (1962) Behaviour of macroscopic rigid spheres in Poiseuille flow Part 2. Experimental results and interpretation. *J Fluid Mech* 14:136–157
- Shao X, Yu Z, Sun B (2008) Inertial migration of spherical particles in circular Poiseuille flow at moderately high Reynolds numbers. *Phys Fluids* 20:103307
- Vasseur P, Cox R (1976) The lateral migration of a spherical particle in two-dimensional shear flows. *J Fluid Mech* 78:385–413
- Zurita-Gotor M, BŁawdziewicz J, Wajnryb E (2007) Swapping trajectories: a new wall-induced cross-streamline particle migration mechanism in a dilute suspension of spheres. *J Fluid Mech* 592:447–469